

Single theoretical model for breakup of viscous thread with and without a fiber

Hyejoon Jun  and Hyoungsoo Kim ^{*}*Department of Mechanical Engineering, Korea Advanced Institute of Science and Technology, Daejeon 34141, South Korea*

(Received 14 January 2024; accepted 25 July 2024; published 20 August 2024)

In this study, we introduce a comprehensive theoretical model for viscous liquid systems exhibiting Rayleigh-Plateau instability, accommodating cases both with and without a solid fiber. Employing the lubrication approach and implementing the hydrodynamic interaction at the solid-liquid interface, we formulate one-dimensional evolution equations for the breakup of viscous liquid threads and films on a fiber. Through several validations, we showed that our model exhibits a good agreement with experimental results in comparison to numerical simulations. Finally, our model, which incorporates the flow effect from the inner boundary condition by reconsidering the ansatz of a conventional long-wave approximation, provides a necessary condition for satellite droplet formation and determines the most unstable mode proportional to k^{*2} , where k^* is the most unstable wavenumber. In addition, we observed that the volume of the satellite droplets exponentially decays depending on the wavenumber. Moreover, our single model integrates the findings of Goren's liquid film on a fiber and Rayleigh's viscous liquid thread, demonstrating its versatility and relevance to a wide range of systems.

DOI: [10.1103/PhysRevFluids.9.084005](https://doi.org/10.1103/PhysRevFluids.9.084005)

I. INTRODUCTION

The Rayleigh-Plateau instability occurs when a liquid column is subjected to capillary forces that cause it to break up into smaller droplets [1]. This instability can occur in ubiquitous natural and man-made systems where cylindrical liquid surfaces are present, such as a stream of water from a faucet [2], dew drops on a spider web [3], rain rivulets on a window [4], gravity-driven thin film drainage along the fiber and the droplet breakup [5–7], and inkjet printing [8,9]. Extensive investigations through various generalizations [1], meticulous experiments [10], molecular dynamics simulations [11,12], and analytical models [13] have been performed. Furthermore, studies advancing universally applicable models by modifying the boundary conditions were conducted, such as the drainage of mobile and immobile soap films [14] and the behavior of instabilities under slip and no-slip conditions [15]. Those studies could provide valuable insights into understanding the phenomena including droplet formation and liquid film breakup across various scenarios. Nonetheless, we think that there is still room to improve the theoretical model of the Rayleigh-Plateau instability.

The challenge associated with the universal model arises from the significantly different breakup modes observed in plug flow [16] and shear flow [17]. In an attempt to address this challenge, Eggers [13] proposed a universal pinch-off curve that drew attention to the presence of satellite droplets in the breakup of visco-inertial liquids. However, this model falls short in explaining the breakup of viscous liquids, as shown in Fig. 1(a), which lacks satellite droplets [1,16]. Additionally,

^{*}Contact author: hshk@kaist.ac.kr

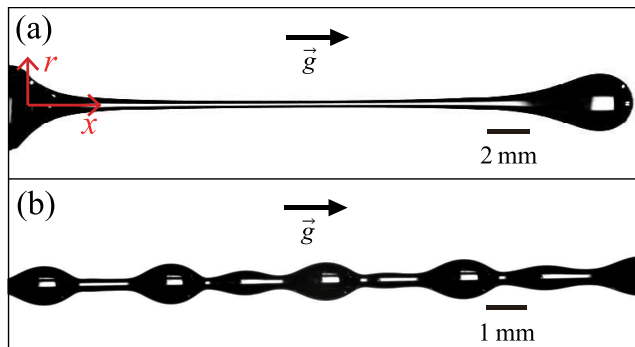


FIG. 1. Examples of Rayleigh-Plateau instabilities. (a) Pinch-off moment of a liquid thread of silicone oil (1000 cSt). (b) Silicone oil (1000 cSt) drops on a fiber. \bar{g} is the gravitational acceleration. See Supplemental Movies 1 and 2 [18].

the presence of a solid fiber in a liquid stream truly alters the interfacial dynamics, as demonstrated in Fig. 1.

When a fiber is present, the resulting breakup of the film becomes periodic, with satellite droplets forming between the primary droplets. In contrast, without the fiber, the viscous thread breaks up into an infinitely long thread without satellite droplets. We think that this instability could be important not only for simple coating [19] but also for the shape of the perturbed liquid film, which plays a significant role in effective water harvesting [20,21] and increasing interfacial shear stress of a fiber in the composite material [22]. However, using a one-dimensional theoretical model framework, the understanding of the hydrodynamic instability of a liquid cylinder, whether with or without a fiber, still remains incomplete. Eventually, we need to ameliorate theoretical models that could explain the formation of satellite droplets in the film on a fiber problem [5,6].

In the meantime, to describe the nonlinear regime of the instability, after an initial linear regime, the long-wave approximation is commonly employed for the breakup of visco-inertial liquid [13] and viscous liquid thread [16]. However, if there is a liquid film on the solid fiber, incorporating the condition at the solid-liquid interface into the long-wave ansatz leads to an inaccurate description of the viscous shear stress in the instability problem. This is because the long-wave ansatz inherently assumes a uniform velocity profile across the film, which fails to capture the nonuniform flow near the solid fiber [17].

To resolve the current issue, literature indicates that due to the geometrical configuration, a different theoretical model must be used depending on the predominant effects among several aspects. Particularly in nonlinear problems, being confined to a simplified conventional long-wave approximation that considered only the first major term inevitably led to the oversight of important effects. Therefore, efforts have been made to include higher-order terms to address more complicated physical situations. For instance, Nayfeh [23] demonstrated that the cutoff wavenumber of instability depends on the initial amplitude of the perturbation by utilizing the second-order term in time expansion, and Tavakol *et al.* [24] addressed that considering higher-order terms enhanced the accuracy of lubrication theory. Consequently, appropriate modification of the ansatz of the long-wave approximation could be conditionally necessary.

In this study, by incorporating the modified long-wave ansatz, we developed a comprehensive one-dimensional theoretical model of the Rayleigh-Plateau instability for viscous liquids, encompassing both cases with and without a fiber based on the lubrication approach and considering the no-slip condition at the fiber surface. Here, we considered a quasistatic situation where the gravitational and convective effects were neglected [25,26]. Using this model, we analytically studied the liquid flow and instabilities, satellite droplet formation, and breakup of the liquid film on a fiber, marking the first instance of such comprehensive analysis within a one-dimensional

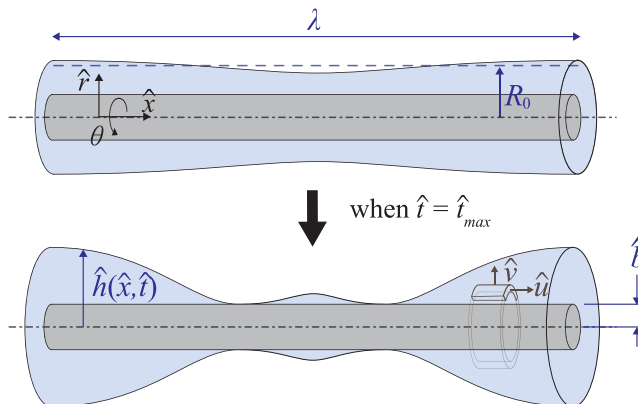


FIG. 2. Schematic of the model problem depicts a single period of a liquid cylinder in cylindrical coordinates $(\hat{r}, \hat{x}, \theta)$, where we could consider that the fiber radius \hat{b} is zero and nonzero. Initially, we used most of the dimensional variables with a hat symbol. Only the basic variables, R_0 , λ , ρ , γ , and μ are without the hat symbol; these indicate the initial radius of the liquid cylinder, wavelength of perturbed surface, fluid density, surface tension, and viscosity, respectively. \hat{h} represents the surface profile and \hat{u} and \hat{v} denote the axial and radial velocities, respectively. After the normalization process, throughout the paper, all variables without the hat symbol ($\hat{\quad}$) represent dimensionless variables.

framework. Furthermore, we unearthed a disregarded condition for satellite droplet formation and obtained a global map of the most unstable mode to be proportional to k^{*2} , where k^* is the most unstable wavenumber. Additionally, we reported that the satellite droplet volume decreases exponentially with increasing wavenumber.

II. ONE-DIMENSIONAL THEORETICAL MODEL

In this study, we considered an axisymmetric cylindrical viscous liquid column with viscosity μ and surface tension γ coaxially coated on a solid fiber. The outer radius of the liquid cylinder is R_0 , and it has a perturbed wavelength of λ , as depicted in Fig. 2. Under this configuration, to simplify the Navier-Stokes equations, we conducted a dimensional analysis using the lubrication theory framework, i.e., $\epsilon (= R_0/\lambda) \ll 1$ [1,27,28]. For nondimensionalization, we employed the viscous timescale and the pressure effect, $\mu R_0/\gamma$ and γ/R_0 , respectively. Here, all variables were expressed in a dimensionless form without using any additional symbol except for the basic variables for the nondimensionalization such as R_0 , λ , ρ , γ , and μ .

Based on the lubrication approximation (i.e., $\epsilon \ll 1$), we adopted the long-wave ansatz of viscous thread, where velocity expands in powers of ϵ^2 [16]. Thus, the radial v and axial u velocity were expressed as $v = v_0 + \epsilon^2 v_1 + \dots$ and $u = (1/\epsilon)(u_0 + \epsilon^2 u_1 + \dots)$, respectively, satisfying continuity. Using this condition, the axisymmetric Stokes equations and the continuity equation yielded

$$0 = -p_x + u_{0xx} + \frac{1}{\epsilon^2 r}(ru_{0r})_r + \frac{1}{r}(ru_{1r})_r, \quad (1)$$

$$0 = -p_r - \frac{v_0}{r^2} + \frac{1}{r}(rv_{0r})_r, \quad (2)$$

$$0 = u_{0x} + \frac{1}{r}(rv_{0r})_r, \quad (3)$$

in the x - r cylindrical coordinates where x denoted the axial coordinate and r denoted the radial coordinate. Here, we considered that the Bond number ($\text{Bo} = \rho g R_0^2/\gamma$) is much less than unity and the Ohnesorge number ($\text{Oh} = \mu^2/\rho\gamma R_0$) is much larger than unity.

For the boundary condition at the free surface at $r = h(x, t)$, we took into account the kinematic condition and the balance of shear and normal stresses, $\vec{n} \cdot \boldsymbol{\sigma} \cdot \vec{n} = -\kappa$ and $\vec{n} \cdot \boldsymbol{\sigma} \cdot \vec{t} = 0$, where h represents the surface profile function, $\boldsymbol{\sigma}$ is the stress tensor, κ is a full curvature of liquid surface, $1/h\sqrt{1 + \epsilon^2 h_x^2} - \epsilon^2 h_{xx}(1 + \epsilon^2 h_x^2)^{-3/2}$, and \vec{n} and \vec{t} are the unit normal and tangential vector on the free surface, respectively. By substituting the velocity series into the boundary conditions, we obtained the following equations at $r = h$:

$$v_0 = h_t + u_0 h_x, \quad (4)$$

$$p_x = -2(h_x u_{0r})_x + 2v_{0rx} + \kappa_x, \quad (5)$$

$$u_{1r} = 2u_{0x} h_x - 2v_{0r} h_x - v_{0x} - \frac{1}{\epsilon^2} u_{0r} + h_x^2 u_{0r}, \quad (6)$$

where higher-order terms in ϵ were neglected. However, the axial curvature $\epsilon^2 h_{xx}$ should be considered to account for the full curvature, as mentioned in previous studies [5, 13, 29, 30]. Therefore, the curvature was simplified as $\kappa \simeq 1/h - \epsilon^2 h_{xx}$. These boundary conditions are consistent with the context of the singular perturbation [5]. From the leading-order term in Eqs. (1) and (6), $u_{0r}(h) = 0$ and $(ru_{0r})_r = 0$, we obtained $u_0 = u_0(x, t)$, which in turn gives $v_0 = u_{0x}(b^2 - r^2)/2r$ from the continuity equation, Eq. (3), and it leads to $p = p(x, t)$ from Eq. (2). Now, we can integrate Eq. (1) twice and substitute $v_0 = u_{0x}(b^2 - h^2)/2h$ into Eq. (4), which gives,

$$u_{1r} = \frac{1}{2}(p_x - u_{0xx})r + \frac{C(x, t)}{r}, \quad (7)$$

$$0 = h_t + u_0 h_x + \frac{1}{2h} u_{0x}(h^2 - b^2), \quad (8)$$

where $C(x, t)$ is the integral constant and we can express the equations in terms of u_0 , h , while u_{1r} and p_x in Eq. (7) would be substituted with Eqs. (5) and (6).

Lastly, we considered the no-slip condition at the solid-liquid interface ($r = b$). Normally, in a one-dimensional model, considering shear stress on the solid fiber under the no-slip condition is challenging. Martínez-Calvo *et al.* [17] pointed out that previous one-dimensional models had failed to accommodate the shear-induced tangential stress due to the uniform velocity profile. In our problem, we used $u_0(x, t)$ as a representative axial velocity which is independent on r . We presumed that the second-order term $u_1(x, r, t)$ was responsible for capturing the shear stress effect along the radial direction in the problem. Neglecting this second-order term at the solid-liquid interface, where the highest shear stress occurred, resulted in the failure of modeling shear-dominant problem. This singular perturbation problem cannot be approximated by setting $\epsilon = 0$, as discussed by Craster and Matar [5].

To resolve this issue, we proposed an extended way of applying the no-slip condition as $u(x, r, t) \simeq (u_0 + \epsilon^2 u_1)/\epsilon = 0$ at $r = b$. Because u_0 was nonzero under unstable flow, the condition addressed that the magnitude of u_1 was assumed to be large enough as close to the solid-liquid interface, while u_1 vanished as $r \rightarrow h$, i.e., $u_1 \simeq -u_0/\epsilon^2$ at $r = b$ and $u_1 = 0$ at $r = h$.

Using the conditions for u_1 , we could reconstruct Eq. (7) so that the no-slip condition was applied as viscous shear stress in the r direction. By organizing Eqs. (7) and (8), we obtained governing equations for the film breakup as

$$u_{0x} \left(3 + \frac{b^2}{h^2} \right) h_x + \frac{u_{0xx}}{2} \left[3h + \left(1 + \frac{b^2}{2h^2} \right) D_{h,b} \right] - \frac{\kappa_x}{4} (2h + D_{h,b}) = -\frac{u_0}{\epsilon^2 h \ln(b/h)}, \quad (9)$$

$$h_t + u_0 h_x + \frac{u_{0x}}{2h} (h^2 - b^2) = 0, \quad (10)$$

where $D_{h,b}$ was a geometric variable of cylinders $\frac{h^2 - b^2}{h \ln(b/h)}$. The one-dimensional evolution equations, $h(x, t)$ and $u_0(x, t)$, for the liquid film breakup can be solved for any dimensionless wavenumber ($k = 2\pi\epsilon$) and fiber radius b .

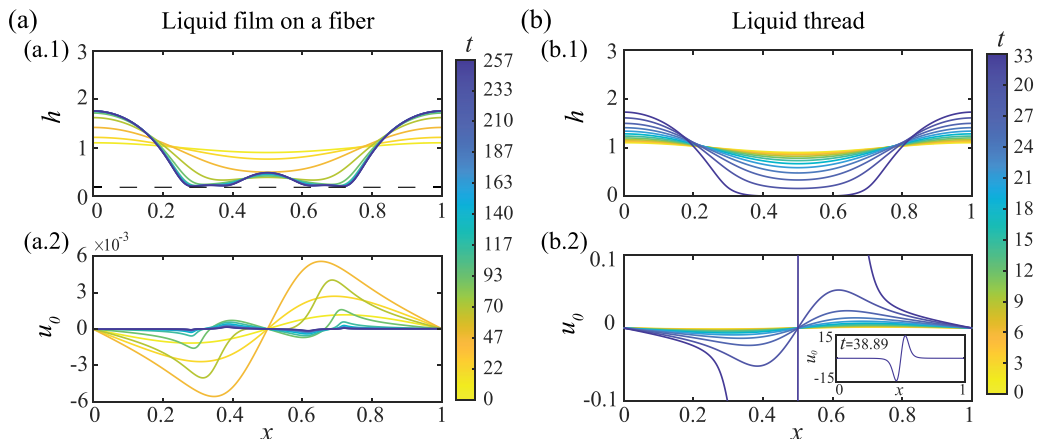


FIG. 3. Time-marching surface profiles h and axial velocity profiles u_0 are shown for (a) the breakup of a film on a solid fiber and (b) the breakup of a viscous liquid thread. The surface profiles are shown in (a.1) and (b.1), while the velocity profiles are shown in (a.2) and (b.2). In (a), $b (= \hat{b}/R_0)$ was set to 0.2, represented as a dashed line in (a.1). In (b.2), the last moment of u_0 was displayed in a small window at the lower right. In all cases, the initial condition was set as a cosine function with a 5% perturbation: $1 + 0.05 \cos(2\pi x)$, and k was set to 0.7. The dimensionless time t ranges from yellow to navy with a total of 12 equally distributed lines.

From the theoretical model, we obtained the time evolution of the surface profile h and axial velocity u_0 for any fiber radius, including the case of fiberless ($b = 0$). Figures 3(a.1) and 3(b.1) demonstrated that for the film on a fiber, a satellite droplet was formed at $x = 0.5$ while the liquid thread was not, which qualitatively well agreed with Fig. 1. A detailed comparison was described in Sec. III.

Not only did we observe satellite droplets, but we also found that the solid surface could retard the interfacial instability, as presented in Fig. 3. For the liquid stream, as h decreased, the Laplace pressure effect dramatically increased, causing faster breakup. However, in the presence of a solid, breakup was delayed as shown in Figs. 3(a.2) and 3(b.2). The dimensionless breakup timescale of the viscous thread without the fiber was about nine times faster than the film on a fiber when $b (= \hat{b}/R_0)$ was 0.2.

The governing equations, Eqs. (9) and (10), were extended to the fiberless case when b went to zero. Therefore, for the fiberless case (i.e., $b \rightarrow 0$, $1/\ln(b) \rightarrow 0$), the governing equations became

$$3u_{0x}h_x + \frac{3}{2}u_{0xx}h - \frac{\kappa_x}{2}h = 0, \quad (11)$$

$$h_t + u_0h_x + \frac{1}{2}u_{0x}h = 0, \quad (12)$$

which resembled Papageorgiou's model for the viscous thread [16], except for the Laplace pressure term where we considered a full curvature profile. In the governing equations, the viscous shear stress effects (i.e., $u/[\epsilon^2 h \ln(b/h)]$) by the solid wall were not included. Thus, the differences between the two cases are anticipated to stem from the influence of viscous shear stress.

III. VALIDATIONS

To validate our model, in Fig. 4, we compared our surface profile results with both the experimental result and the two-dimensional numerical simulation result from the previous study [25].

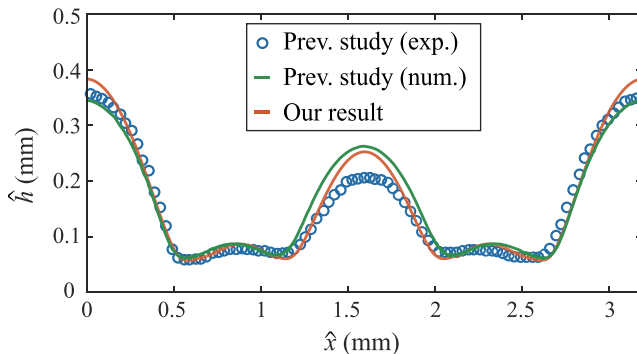


FIG. 4. Comparison of our calculated surface profile from the theoretical model (the red line) with the previous experimental results (blue hollow symbols) and numerical simulation results (the green line) of Gonzalez *et al.* [25]. The wavelength and initial film outer radius were set to be equal, and the amplitude was set to 0.05.

To compare the results fairly, we extracted the information from the literature and the results were normalized with each variable, accordingly. So, here, the hat symbol ($\hat{\cdot}$) was used for the dimensional variables to distinguish them from the dimensionless variables.

For the validation, the geometric conditions were used, such as the wavelength of the instability $\lambda = 3.19$ mm, liquid radius $R_0 = 0.19$ mm, and fiber radius $\hat{b} = 0.055$ mm, to obtain dimensionless values of $b = 0.288$ and $k = 0.376$ for our dimensionless governing equations. In Fig. 4, our result (the red line) showed a good agreement with the experimental result (the blue hollow symbols) and the numerical result (the green line). For the quantitative comparison, discrepancy of the surface profile was calculated by measuring the surface difference at each point (see further details about the quantification of the discrepancy in Sec. S1 of the Supplemental Material [18]). Our model showed the discrepancy of 9.8%, which was 30% less than that of the literature's results done by numerical simulation (14.1%). This result indicates that our model could be useful to investigate the droplet breakup of the viscous liquid thread with a relatively better accuracy.

Additionally, we compared our results with two-dimensional numerical simulation results by Mashayek and Ashgriz [31], considering various values of b when the Ohensorge number ($\text{Oh} = \mu^2/\rho\gamma R_0 \gg 1$). In this case, we considered viscous liquid for $\text{Oh} = 100$, the dimensionless wavenumber $k (= 2\pi R_0/\lambda) = 0.5$, and the dimensionless fiber radii $b = 0.1, 0.3$, and 0.5 , which were the same conditions of the literature [31]. The initial condition was set as $(1 - A^2/2) + A \cos(kz)$ where the amplitude of disturbance is set to $A = 0.05$.

Figure 5(a) illustrated half of a single periodic surface, with the left small bump indicating the presence of a satellite droplet and the right, larger bump representing the mother droplet. The current theoretical model captured the major features, such as the position of the neck, the presence of the subsatellite droplet as well as the satellite droplet and the volume difference were compared in Fig. 5(b).

For the quantitative comparison, in Fig. 5(a), the discrepancy with the two-dimensional simulation was calculated as 15.1%, 5.8%, and 3.7% when b values were 0.1, 0.3, and 0.5, respectively. This discrepancy increased as the b value decreased, especially near the mother droplet on the right-hand side, where the surface slope was higher. These differences can be attributed to simplifications made during the modeling process, particularly in the treatment of the pressure term. Specifically, when considering the Laplace pressure term, we assumed $\sqrt{1 + \epsilon^2 h_x^2} \sim 1$, causing an overestimation of pressure at inclined surfaces compared to the numerical results. Only to check this effect, we modified the Laplace pressure term using the full curvature relation although the approximation does not satisfy this. We observed that the modified Laplace pressure case provided

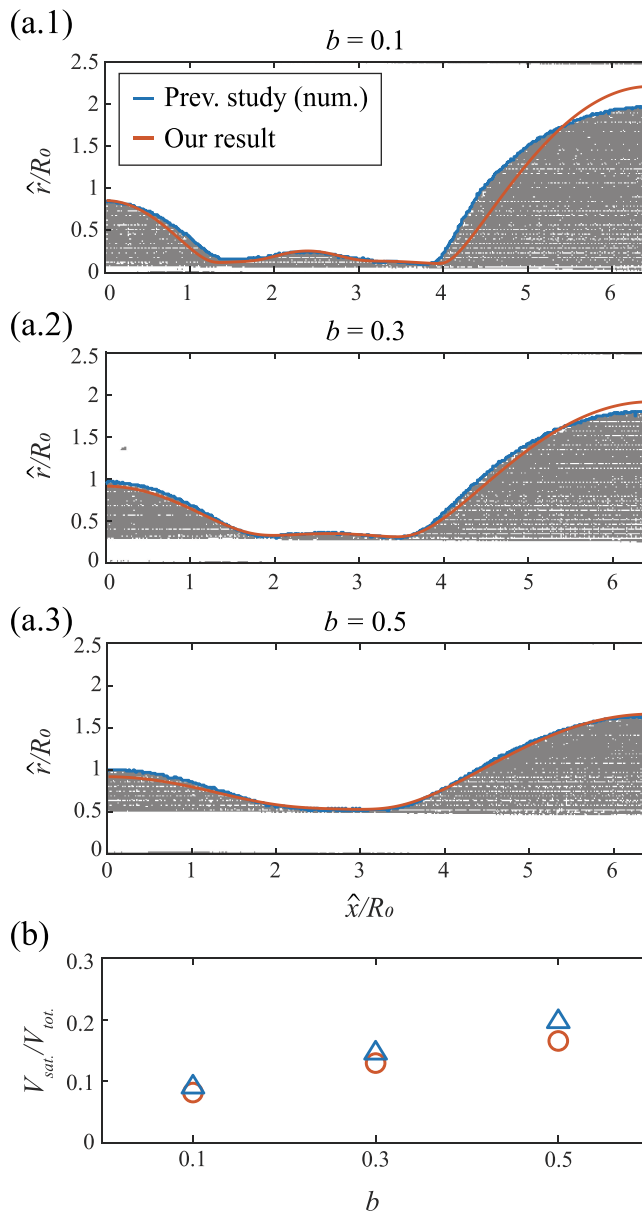


FIG. 5. Validation with two-dimensional simulation of Mashayek's previous work when the dimensionless fiber radii b are 0.1 for (a.1), 0.3 for (a.2), and 0.5 for (a.3), respectively. (b) Satellite droplet volume to total liquid volume of our results (\circ) and simulation results (Δ) for $b = 0.1, 0.3$, and 0.5 . The blue and red colors indicate the Mashayek's simulation results and the current results from our model, respectively.

a better prediction, especially for $b = 0.1$ and 0.3 (see more details in Sec. S2 of the Supplemental Material [18]). Under this circumstance, at the moment, we admit that the lubrication approximation in the one-dimensional theoretical model is somewhat limited. Nonetheless, we believe that the current model provides a reasonably good agreement with the literature, both with and without a fiber.

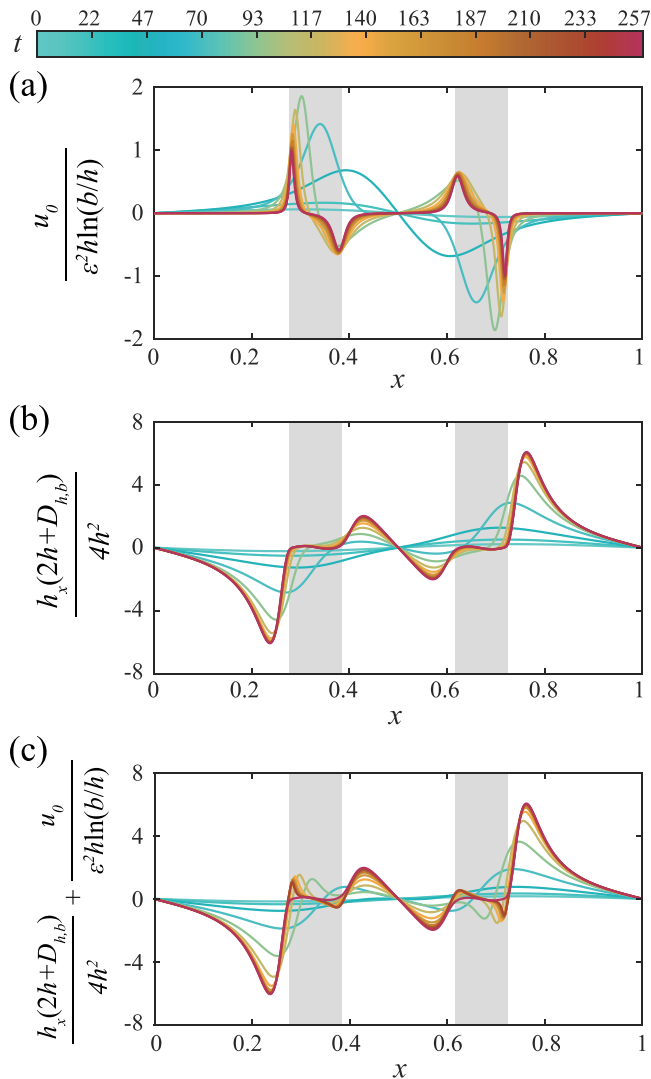


FIG. 6. Time evolution of (a) the viscous shear stress effect, $u_0/[\epsilon^2 h \ln(b/h)]$, (b) the Laplace pressure effect, $h_x(2h + D_{h,b})/4h^2$, in Eq. (9), where $D_{h,b} = (h^2 - b^2)/[h \ln(b/h)]$, and (c) the difference between the viscous shear stress and the Laplace pressure gradient are presented. The change in dimensionless time t is indicated by the colorbar ranging from cyan to red until the liquid breaks up ($t = 257$). The gray region indicates that viscous shear stress is relatively dominant, while the Laplace pressure effect is less dominant. The calculated case corresponds to $b = 0.2$ and $k = 0.7$.

IV. SATELLITE DROPLET FORMATION BY VISCOUS SHEAR STRESS

The dynamics of the breakup of a viscous liquid was determined not only by the capillary force acting on a liquid surface but also by the viscous effect as mentioned by Rayleigh [1]. In our problem, we eventually found that the viscous shear stress $u/[\epsilon^2 h \ln(b/h)]$ from the solid fiber was crucial for the formation of a satellite droplet and the delay of the breakup, as shown in Figs. 1 and 3.

To address this hydrodynamic effect, we presented and compared the viscous shear stress term and Laplace pressure term, as shown in Fig. 6. From the sign change of each term, we could interpret

that the Laplace pressure effect induced the flow outward from the neck (the gray region in Fig. 6) where the local h was at its minimum or where $h_x = 0$ and $u_0 = 0$, while the viscous shear stress effect restrained the fluid motion. At the beginning point of the instability, the viscous shear stress forced liquid to flow to the center point ($x = 0.5$) making an initial bump at the center, as indicated by the cyan color lines of Fig. 6. After a small bump was formed, the positions of the neck would be changed, and Laplace pressure caused the liquid to flow towards the outside of the new necks, generating satellite droplets. In the meantime, because of viscous shear stress, liquid flowed to the changed necks which were in the gray area, thereby delaying the breakup time.

The effect of viscous shear stress was usually lower than that of Laplace pressure, but near the neck indicated as the gray region, the viscous shear stress was more dominant. In this region, the viscous shear stress effect mostly showed the local extremum but the Laplace pressure effect became minor. Thus, the viscous shear stress was dominant in the gray area, as shown in Fig. 6(c), which induced the droplet formation.

V. DROPLET BREAKUP MECHANISM BY HYDRODYNAMIC EFFECT AT THE SOLID-LIQUID INTERFACE

It is well known that the mechanism of satellite droplet formation is sensitive not only to the geometry of the fiber [10], but also to the hydrodynamic effect (i.e., slip or no-slip) at the solid-liquid interface [15,32]. Thus, to fully understand the breakup mechanism, it is important to manage the interaction at the solid-liquid interface. To consider a slip effect, we implemented the effect of the viscous stress as a boundary condition, which enabled one to adjust the degree of the interaction between liquid and solid.

In the derivation process of the governing equations, we knew that the amount of slip effect on a fiber was related to the velocity ratio of u_1 to u_0 , so the slip parameter can be defined as $\alpha_{\text{slip}} \equiv -\epsilon^2 u_1 / u_0$. Namely, the no-slip condition corresponded to $u_1 / u_0 = -1 / \epsilon^2$ and the total slip condition corresponded to $u_1 / u_0 = 0$, since $u(x, r, t) \simeq (u_0 + \epsilon^2 u_1) / \epsilon$. By utilizing this parameter, the viscous stress term in Eq. (9) could be modified as $-\alpha_{\text{slip}} u_0 / [\epsilon^2 h \ln(b/h)]$.

The slip parameter α_{slip} was correlated with the dimensionless slip length ($L_{\text{slip}} = \hat{L}_{\text{slip}} / R_0$) used in the Navier-slip condition, where \hat{L}_{slip} is the hydrodynamic slip length of the fiber surface. Therefore, here, $L_{\text{slip}} = 0$ for $\alpha_{\text{slip}} = 1$ and $L_{\text{slip}} = \infty$ for $\alpha_{\text{slip}} = 0$. Based on this, we defined α_{slip} as an ansatz, $\alpha_{\text{slip}} = 1 / (1 + L_{\text{slip}} / h)$, where h matched the nondimensionalization parameter used in the literature on the strong-slip regime [33]. This relation is reasonable because the slip length reduces the viscous stress by an amount proportional to the increased length, modifying it from $-u_0 / [\epsilon^2 h \ln(b/h)]$ to $-u_0 / [\epsilon^2 (h + L_{\text{slip}}) \ln(b/h)]$. Then, the governing equations with the Navier-slip condition became

$$u_{0x} \left(3 + \frac{b^2}{h^2} \right) h_x + \frac{u_{0xx}}{2} \left[3h + \left(1 + \frac{b^2}{2h^2} \right) D_{h,b} \right] - \frac{\kappa_x}{4} (2h + D_{h,b}) = -\frac{u_0 / \epsilon^2}{(h + L_{\text{slip}}) \ln(b/h)}, \quad (13)$$

$$0 = h_t + u_0 h_x + \frac{u_{0x}}{2h} (h^2 - b^2). \quad (14)$$

In Fig. 7, we presented h and u_0 for the same values of $b = 0.2$ and $k = 0.7$ for the no-slip ($L_{\text{slip}} = 0$) and Navier-slip boundary conditions of strong slip with $L_{\text{slip}} = 10$ and 100. Our results extended from the no-slip condition to the strong-slip regime, where the dewetting feature was known to be dramatically different [15,32]. The results demonstrated a significant reduction in viscous effects near the solid-liquid interface of the solid fiber, decreasing the breakup time by more than fourfold and potentially reducing the size of satellite droplets to negligible levels, as previously reported [32]. As the dimensionless slip length increased by a factor of 10, in Fig. 7(c), the breakup time slightly decreased and the magnitude of u_0 slightly increased. Differences between slip and no-slip results can be attributed to the decrease in viscous shear stress exerted by the solid surface by a factor of L_{slip} / h , which would otherwise impede liquid flow particularly in the vicinity of the solid

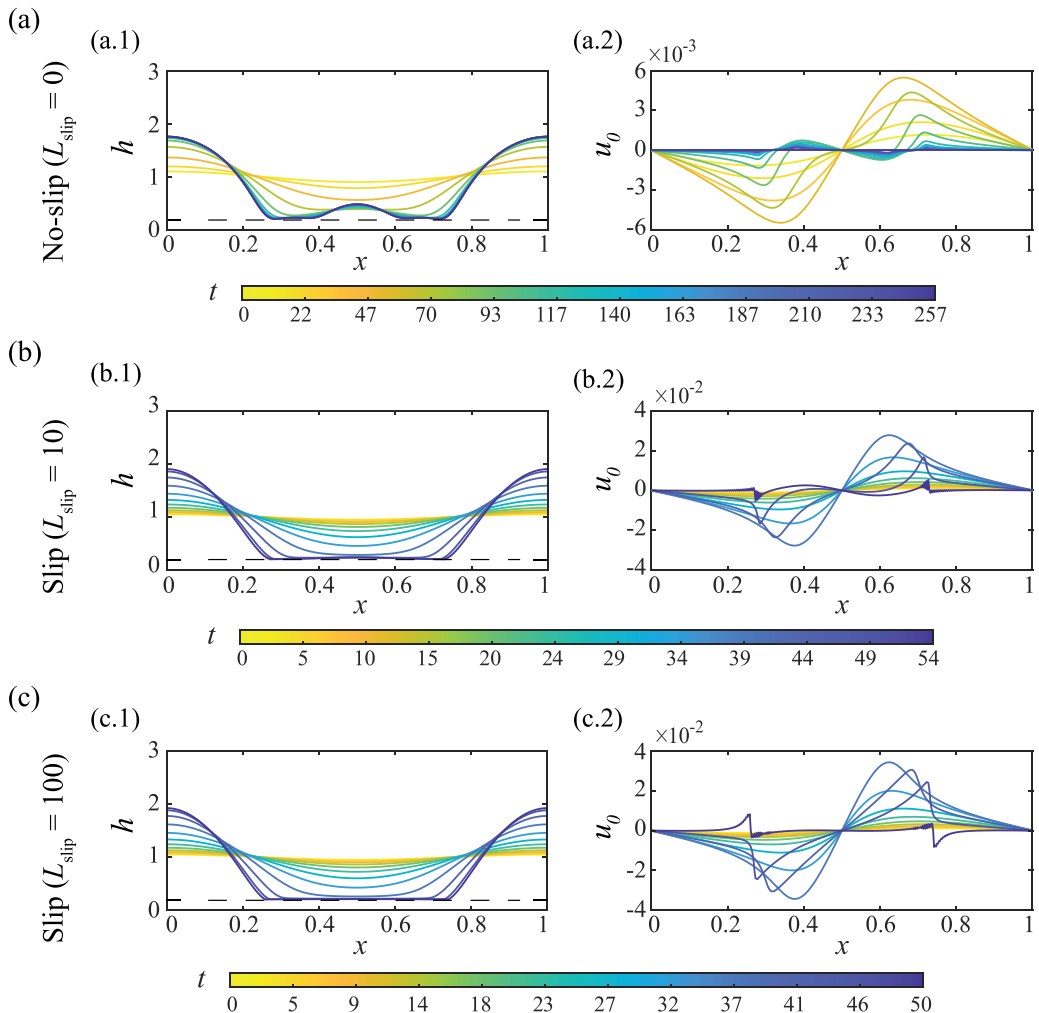


FIG. 7. Time-marching surface profile function h and axial velocity function u_0 during the breakup of a liquid film on a solid fiber under two different conditions: (a) no-slip condition and slip condition when (b) $L_{\text{slip}} = 10$ and (c) $L_{\text{slip}} = 100$. The surface profiles are shown in (a.1), (b.1), and (c.1), while the velocity profiles are shown in (a.2), (b.2), and (c.2). For all cases, the initial condition was set as a cosine function with a 5% perturbation: $1 + 0.05 \cos(2\pi x)$. The values of k and b were set to 0.7 and 0.2, respectively, where dashed lines represent the fiber surface in (a.1), (b.1), and (c.1). When L_{slip} were 0, 10, and 100, the breakup times were 257, 54, and 50, in the dimensionless timescale, respectively.

surface where h was close to b . Overall, our results highlighted the importance of considering the hydrodynamic effect, i.e., viscous shear stress for dewetting [32], enabling a more comprehensive analysis of the classical Rayleigh-Plateau instability problem in a wide variety of situations.

VI. ANALYSIS ON THE BREAKUP OF THE VISCOUS LIQUID THREAD WITH AND WITHOUT A FIBER

We presented that the current single model enabled the investigation of a viscous liquid column with and without a fiber. To test the effect of the geometry between the fiber size and liquid film thickness, we extensively investigated the Rayleigh-Plateau instabilities at various b values,

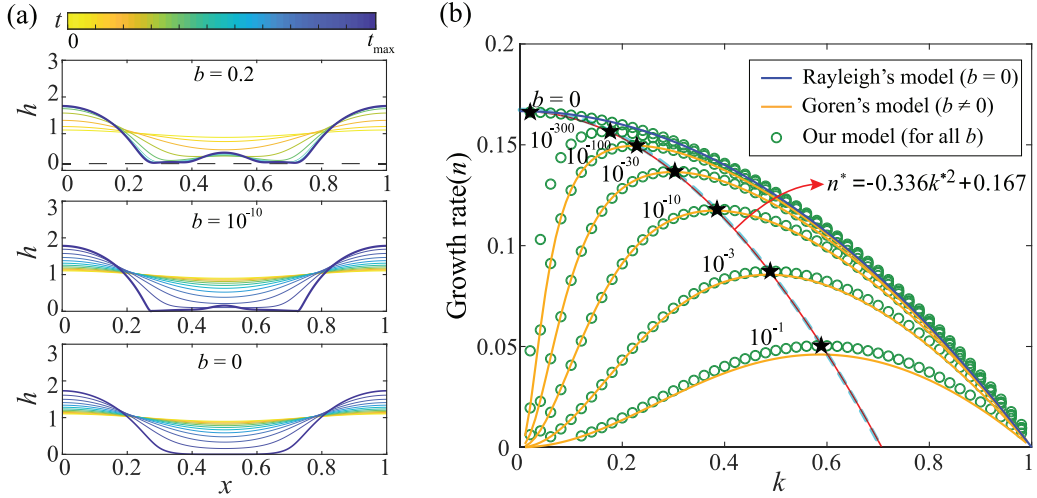


FIG. 8. (a) Comparison of liquid surface profiles for different values of b ($= 0.2, 10^{-10}$, and 0) while keeping k fixed at 0.7. Here, t_{\max} is the breakup moment and it was 257, 37, and 32 when the values of b were 0.2, 10^{-10} , and 0, respectively. The black dashed lines represent the fiber surface. (b) Dispersion relations showing the growth rate n of b ranging from 10^{-1} to 0. The most unstable growth rates k^* (the black stars) were fitted along the black dashed line, $n^* = -0.336k^{*2} + 0.167$, which is the red solid line. Our results (the green circles) were compared with previous research results. The blue and orange lines represent Rayleigh's and Goren's theoretical results [1,28], respectively, and the cyan dashed line indicates the graph of Rayleigh's model reduced by a factor of $\sqrt{2}$ in the k direction.

including even $b = 0$. Figure 8(a) showed the representative results of the effect of the fiber radius b and presented the film profiles h for $b = 0.2, 10^{-10}$, and 0. The results clearly demonstrated that even for extremely small values of b ($= 10^{-10}$), the presence of a fiber resulted in the formation of satellite droplets, and the size of these satellite droplets decreased as b decreased. We could observe this phenomena by implementing the viscous shear stress, $u_0/[\epsilon^2 h \ln(b/h)]$, in the model. If h approached b right before the film breakup, the viscous term was approximated as $u_0(h/b)/(h-b) \simeq u_0/(h-b)$. Therefore, in this case regardless of the value of b , the viscous effect became dominant, namely, making the formation of satellite droplets inevitable.

Finally, we calculated the growth rate n for most of the b values covering from 10^{-1} to 0 at each k and b . The results were plotted as the green circles, as shown in Fig. 8(b). From this result, we observed that the dependency on the logarithmic value of b affected the growth rate n and the most unstable wavenumber k^* , representing the wavenumber where n was at its maximum. We think that the growth rate relation is highly dependent on the viscous effect because the viscous term $u_0/[\epsilon^2 h \ln(b/h)]$ could be approximated as $u_0/|\ln b|$ when the liquid surface was comparable to the initial radius R_0 ($h = \hat{h}/R_0 \simeq 1$, where \hat{h} is the dimensional surface profile). For the validation, in Fig. 8(b), we overlaid literature results of the representative analytical studies, where the blue and orange solid lines indicated the predictions by Rayleigh [1] and Goren [28], respectively. In Fig. 8(b), a comparison between our model and the previous model showed an excellent agreement for all the b values. Although Rayleigh's solution focused solely on liquid thread breakup and Goren's solution diverged at $b = 0$, virtually, our model consolidated both solutions into a single framework.

Additionally, we determined the k^* ($= 2\pi R_0/\lambda^*$), highlighted as the black stars, in Fig. 8(b), indicating the spatial periodicity [1,27,28]. Figure 8(b) showed that the k^* value for the liquid film on a fiber ($b > 0$) gradually approached zero as $b \rightarrow 0$. Notably, we found that the most unstable growth wavenumber k^* followed a quadratic function (the red solid line) for all b , namely, $n^* =$

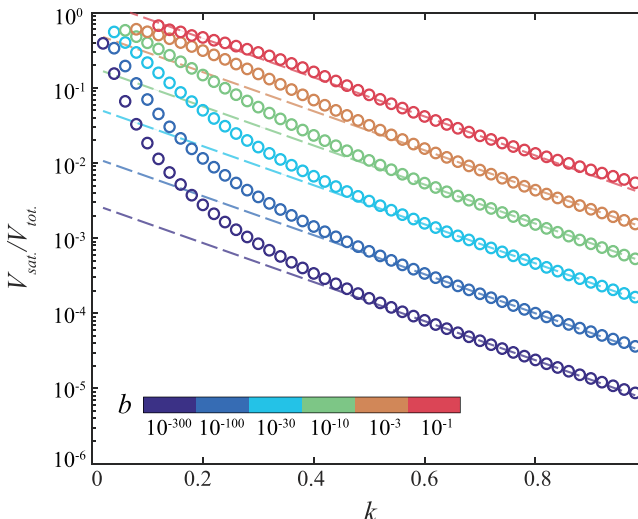


FIG. 9. Satellite droplet volume normalized by its total volume depending on b ranges from 10^{-300} to 10^{-1} . Dashed lines are fitted lines with a slope of -2.6 on a log-linear scale.

$-0.336k^{*2} + 0.167$. As mentioned, n is determined by the early regime of the instability, which is related to viscous shear stress, $u_0/[\epsilon^2 h \ln(b/h)]$, approximated as $1/[\epsilon^2 |\ln(b)|]$. This in turn is related to k^2 and the logarithmic of b . Interestingly, this quadratic relation showed that the (k^*, n^*) graph coincided with the growth rate of a viscous thread divided by $\sqrt{2}$, denoted as $(k_0/\sqrt{2}, n_0)$ [1] aligning with the previous expectation that k^* is $1/\sqrt{2}$ when $b \simeq 1$ [26,34].

For the Rayleigh-Plateau instability problem, another interesting point could be the size of the satellite droplets. In a previous study, Martínez-Calvo *et al.* [17] showed that the volume followed a power-law trend depending on the Laplace number. Here, using our model, we investigated the effect of the wavenumber k on the size of the satellite droplets, where the satellite volume was normalized by the total volume for the comparison, $\pi(R_0^2 - b^2)\lambda$ (Fig. 9). As the wavenumber k approached zero (i.e., $\lambda \rightarrow \infty$), the satellite droplet volume increased and converged to unity for all cases, indicating that viscous shear stress restrained flow toward a mother droplet. For large values of k , there was a reduction in the satellite droplet volume, which showed an exponential decay trend, which had not been observed before.

VII. CONCLUSION AND OUTLOOK

To date, a one-dimensional theoretical model for the Rayleigh-Plateau instability has not been able to predict the droplet breakup phenomena due to the lack of consideration for the shear stress effect along the r direction because of conventional simplifications [17,35]. In this study, we have demonstrated comprehensive one-dimensional evolution equations for the breakup of a viscous liquid encompassing both with and without a fiber case by implementing the suggested inner boundary condition with the second largest term in the ansatz. In this case, we found that the second largest term $u_1(x, r, t)|_{r \rightarrow b}$ is physically meaningful near the solid-liquid interface for applying the viscous shear from the fiber, following $u_1/u_0 \sim 1/\epsilon^2$.

The current model, an extension of Papageorgiou's [16] theoretical framework for viscous liquid threads, underwent validation through theoretical, experimental, and numerical results. In the range where the dimensionless fiber radius b varies from 10^{-1} to 0, we integrated two distinct theoretical approaches concerning the early stages of instability, drawing from the growth rates proposed by Rayleigh [1] and Goren [28]. Furthermore, we compared the breakup of the

liquid film with the experimental and numerical results from Gonzalez [25] and the numerical findings of Mashayek and Ashgriz [31], demonstrating excellent agreement for the late stage of the instability.

Based on our findings, we anticipate that it will provide physical insights into the mechanisms governing thin film breakup phenomena, including the formation of satellite droplets, changes in periodicity, and the effects of surface slip. Through the unified model for both viscous threads and films on a fiber, we analyzed the Rayleigh-Plateau instability of viscous liquids, showing significant variations depending on the presence of a fiber. The results attributed to the boundary condition were due to the shear stress effect. From the results at various values of b and k , we observed that the fastest growth rate mode and the satellite droplet volume are functions of the wavenumber, with $n^* \sim -k^2$ and $V_{\text{sat}}/V_{\text{tot}} \sim \exp(k)$, respectively.

As we extended the problem from viscous thread to film on a fiber and also introduced the hydrodynamic effect in terms of viscous shear stress at the solid-liquid interface regarding the slip effect, these ideas could be applied to investigate other breakup problems involving satellite droplets and periodicity. For example, when considering additional factors such as inertia [13], surface viscosity from surfactants [36], hydrodynamic effects [15], and shear stress from a surrounding liquid [27], our framework may provide further understanding of breakup dynamics across various contexts. Furthermore, given Goren's model's success in explaining the nucleation position of small microtubules in Setru's study [3], we anticipate that phenomena like the "beads on a string" case [37] occurring in polymer solutions or viscous liquid containing short nanofibers could also be analyzed through our model, particularly in cases with a very small fiber radius.

ACKNOWLEDGMENTS

This work was supported by Basic Science Research Program through the National Research Foundation of Korea funded by the Ministry of Science (Grant No. NRF-2021R1A2C2007835).

-
- [1] L. Rayleigh, On the instability of cylindrical fluid surfaces, *London, Edinburgh, Dublin Philos. Mag. J. Sci.* **34**, 177 (1892).
 - [2] V. Grubelnik and M. Marhl, Drop formation in a falling stream of liquid, *Am. J. Phys.* **73**, 415 (2005).
 - [3] S. U. Setru, B. Gouveia, R. Alfaro-Aco, J. W. Shaevitz, H. A. Stone, and S. Petry, A hydrodynamic instability drives protein droplet formation on microtubules to nucleate branches, *Nat. Phys.* **17**, 493 (2021).
 - [4] J. A. Diez, A. G. González, and L. Kondic, On the breakup of fluid rivulets, *Phys. Fluids* **21**, 082105 (2009).
 - [5] R. V. Craster and O. K. Matar, On viscous beads flowing down a vertical fibre, *J. Fluid Mech.* **553**, 85 (2006).
 - [6] C. Duprat, C. Ruyer-Quil, S. Kalliadasis, and F. Giorgiutti-Dauphiné, Absolute and convective instabilities of a viscous film flowing down a vertical fiber, *Phys. Rev. Lett.* **98**, 244502 (2007).
 - [7] H. Ji, A. Sadeghpour, Y. S. Ju, and A. L. Bertozzi, Modelling film flows down a fibre influenced by nozzle geometry, *J. Fluid Mech.* **901**, R6 (2020).
 - [8] Y. Zhang, G. Hu, Y. Liu, J. Wang, G. Yang, and D. Li, Suppression and utilization of satellite droplets for inkjet printing: A review, *Processes* **10**, 932 (2022).
 - [9] Q. Yang, H. Li, M. Li, Y. Li, S. Chen, B. Bao, and Y. Song, Rayleigh instability-assisted satellite droplets elimination in inkjet printing, *ACS Appl. Mater. Interfaces* **9**, 41521 (2017).
 - [10] J. Eggers and E. Villermaux, Physics of liquid jets, *Rep. Prog. Phys.* **71**, 036601 (2008).
 - [11] J. Koplik and J. R. Banavar, Molecular dynamics of interface rupture, *Phys. Fluids* **5**, 521 (1993).
 - [12] C. Zhao, J. E. Sprittles, and D. A. Lockerby, Revisiting the Rayleigh-Plateau instability for the nanoscale, *J. Fluid Mech.* **861**, R3 (2019).

- [13] J. Eggers, Universal pinching of 3D axisymmetric free-surface flow, *Phys. Rev. Lett.* **71**, 3458 (1993).
- [14] L. W. Schwartz and R. V. Roy, Modeling draining flow in mobile and immobile soap films, *J. Colloid Interface Sci.* **218**, 309 (1999).
- [15] S. Haefner, M. Benzaquen, O. Bäümchen, T. Salez, R. Peters, J. D. McGraw, K. Jacobs, E. Raphaël, and K. Dalnoki-Veress, Influence of slip on the Plateau–Rayleigh instability on a fibre, *Nat. Commun.* **6**, 7409 (2015).
- [16] D. T. Papageorgiou, On the breakup of viscous liquid threads, *Phys. Fluids* **7**, 1529 (1995).
- [17] A. Martínez-Calvo, J. Rivero-Rodríguez, B. Scheid, and A. Sevilla, Natural break-up and satellite formation regimes of surfactant-laden liquid threads, *J. Fluid Mech.* **883**, A35 (2020).
- [18] See Supplemental Material at <http://link.aps.org/supplemental/10.1103/PhysRevFluids.9.084005> for further details on the movies about the breakup of the liquid column and the validation of our model with modification of Laplace pressure.
- [19] M. Hamadiche and H. Abou-Shady, Optical fiber instability during coating process, *J. Fluids Struct.* **22**, 599 (2006).
- [20] L. Shang, F. Fu, Y. Cheng, Y. Yu, J. Wang, Z. Gu, and Y. Zhao, Bioinspired multifunctional spindle-knotted microfibers from microfluidics, *Small* **13**, 1600286 (2017).
- [21] Y. Zheng, H. Bai, Z. Huang, X. Tian, F.-Q. Nie, Y. Zhao, J. Zhai, and L. Jiang, Directional water collection on wetted spider silk, *Nature (London)* **463**, 640 (2010).
- [22] C. W. Rodricks, I. Greenfeld, B. Fiedler, and H. D. Wagner, Fragmentation of beaded fibres in a composite, *Materials* **15**, 890 (2022).
- [23] A. H. Nayfeh, Nonlinear stability of a liquid jet, *Phys. Fluids* **13**, 841 (1970).
- [24] B. Tavakol, G. Froehlicher, D. P. Holmes, and H. A. Stone, Extended lubrication theory: Improved estimates of flow in channels with variable geometry, *Proc. R. Soc. A* **473**, 20170234 (2017).
- [25] A. G. Gonzalez, J. A. Diez, R. Gratton, D. M. Campana, and F. A. Saita, Instability of a viscous liquid coating a cylindrical fibre, *J. Fluid Mech.* **651**, 117 (2010).
- [26] S. L. Goren, The shape of a thread of liquid undergoing break-up, *J. Colloid Sci.* **19**, 81 (1964).
- [27] S. Tomotika, On the instability of a cylindrical thread of a viscous liquid surrounded by another viscous fluid, *Proc. R. Soc. A* **150**, 322 (1935).
- [28] S. L. Goren, The instability of an annular thread of fluid, *J. Fluid Mech.* **12**, 309 (1962).
- [29] B. Ambravaneswaran and O. A. Basaran, Effects of insoluble surfactants on the nonlinear deformation and breakup of stretching liquid bridges, *Phys. Fluids* **11**, 997 (1999).
- [30] F. J. García and A. Castellanos, One-dimensional models for slender axisymmetric viscous liquid jets, *Phys. Fluids* **6**, 2676 (1994).
- [31] F. Mashayek and N. Ashgriz, Instability of liquid coatings on cylindrical surfaces, *Phys. Fluids* **7**, 2143 (1995).
- [32] D. Peschka, S. Haefner, L. Marquant, K. Jacobs, A. Münch, and B. Wagner, Signatures of slip in dewetting polymer films, *Proc. Natl. Acad. Sci. USA* **116**, 9275 (2019).
- [33] A. Münch, B. Wagner, and T. P. Witelski, Lubrication models with small to large slip lengths, *J. Eng. Math.* **53**, 359 (2005).
- [34] D. Quéré, Fluid coating on a fiber, *Annu. Rev. Fluid Mech.* **31**, 347 (1999).
- [35] J. A. Diez and L. Kondic, On the breakup of fluid films of finite and infinite extent, *Phys. Fluids* **19**, 072107 (2007).
- [36] H. Wee, B. W. Wagoner, P. M. Kamat, and O. A. Basaran, Effects of surface viscosity on breakup of viscous threads, *Phys. Rev. Lett.* **124**, 204501 (2020).
- [37] R. Sattler, S. Gier, J. Eggers, and C. Wagner, The final stages of capillary break-up of polymer solutions, *Phys. Fluids* **24**, 023101 (2012).